

RESEARCH

Open Access



Exploring the mitigating potential of anthocyanin Malvidin in a mouse model of bleomycin-induced pulmonary fibrosis by inhibiting NLRP3 inflammasome activation and oxidative stress

Dingzi Zhou¹, Lin Cai¹, Jie Xu¹, Daigang Fu¹, Ling Yan¹ and Linshen Xie^{1*}

Abstract

Background Malvidin (MV), an essential anthocyanin, has antioxidant and anti-inflammatory effects that may help treat pulmonary fibrosis (PF), a progressive and occasionally fatal condition characterized by severe lung scarring, oxidative stress, and inflammation.

Objective This study aims to evaluate the therapeutic potential of MV in PF by assessing its effects on inflammation, oxidative stress, and fibrotic markers through in vitro and in vivo models.

Methods and materials The compound was evaluated by molecular docking. BEAS-2B and RLE-6TN cells were treated with 200 µg/mL BLM to induce inflammation, followed by MV treatment. Cell viability, ROS levels, and wound healing were analyzed. In vivo, BLM-induced mice were evaluated to assess fibrotic and antioxidant biomarkers.

Results MV interacted with NLRP3 with a binding energy of -7 kcal/mol. MV increased cell viability in BLM-induced cells, reducing ROS and oxidative stress. Wound healing was enhanced in MV-treated groups. A decrease in HYP proteins confirms MV's antifibrotic effects. In the mice model, MV reduced TXNIP, MDA, and MPO while increasing CAT, GSH, and SOD, confirming its antioxidant capacity.

Conclusion MV alleviated PF in the BLM-induced model via the NLRP3 inflammasome pathway, demonstrating its potential as an antifibrotic and antioxidant agent.

Keywords Malvidin, NLRP3, Bleomycin, Fibrosis, Inflammation, Oxidative stress

*Correspondence:

Linshen Xie
drxiels@sina.com

¹West China School of Public Health and West China Fourth Hospital, Sichuan University, Chengdu 610041, China



© The Author(s) 2025. **Open Access** This article is licensed under a Creative Commons Attribution-NonCommercial-NoDerivatives 4.0 International License, which permits any non-commercial use, sharing, distribution and reproduction in any medium or format, as long as you give appropriate credit to the original author(s) and the source, provide a link to the Creative Commons licence, and indicate if you modified the licensed material. You do not have permission under this licence to share adapted material derived from this article or parts of it. The images or other third party material in this article are included in the article's Creative Commons licence, unless indicated otherwise in a credit line to the material. If material is not included in the article's Creative Commons licence and your intended use is not permitted by statutory regulation or exceeds the permitted use, you will need to obtain permission directly from the copyright holder. To view a copy of this licence, visit <http://creativecommons.org/licenses/by-nc-nd/4.0/>.

Introduction

Pulmonary fibrosis (PF) is a condition characterized by injury and scarring in the lungs, which makes breathing difficult due to the lung's inability to carry oxygen to the bloodstream [1]. In PF, the normal lung tissue morphology was replaced by scar tissue, which may also lead to the accumulation of collagen deposition and fibroblast proliferation [2]. There is a high death rate in PF Patients, and the survival rate is two to three years following diagnosis. The way the disease worked wasn't clear, but it involved persistent micro-injuries caused by PF, activation of alveolar epithelial cells, and abnormal alveolar repair [3]. The lung's interstitium and alveolar epithelial cells trigger an abnormally high production of oxidative stress factors and pro-fibrotic mediators like inflammatory cytokines [4]. Despite significant efforts to develop a treatment for PF, only two approved drugs, pirfenidone and nintedanib, are available. While they help reduce inflammation, they do not provide a permanent cure [5]. Hence, the lung disease known as PF has a potentially fatal prognosis and a negligible response to current medical treatments [6]. To overcome this drawback, there is the urge to develop a drug that provides permanent recovery, and it also tends to be non-toxic with fewer side effects. A few drugs are commercially available to induce fibrosis, such as bleomycin (BLM), which has been widely used in both cell lines and animal models. The active component in BLM may induce oxidative stress and elevate ROS levels, potentially contributing to fibrotic conditions [7]. Therefore, researchers selected BLM as a universal drug capable of inducing fibrosis, based on a well-defined mechanism of its action [8]. Additionally, they increase HIF-1 α levels and alter the composition of bronchoalveolar lavage fluid (BALF), indicating that HIF-1 α stabilization contributes to the progression of PF and that HIF-1 α inhibition may serve as a promising therapeutic strategy for PF [9].

Anthocyanin is a class of water-soluble flavonoids commonly present in fruits, red wines, and other foods. Malvidin (MV) is one of the six most prominent anthocyanins and a member of the O-methylated anthocyanidin family. The MV's solubility in water is higher than that of methanol and ethanol. Red wines, fruits, and the skin of red grapes are rich sources of MV, also known as malvidin-3-glucoside [10, 11]. They have antioxidants, anti-hypertension, anti-osteoarthritis, anti-inflammatory, and anti-proliferative properties. They also possess cytotoxic effects against some cancer cells [12]. MV can lower reactive oxygen species (ROS), raise superoxide dismutase (SOD) levels, and participate in the pathways that lower inflammation. A natural grape product is used in treatment to lessen the negative effects of these drugs. In our present study, MV has been found to have a better effect against the pyrin domain-containing 3 (NLRP3) pathway

to reduce PF, as determined by docking analysis. Previous studies have stated that the inflammasome complex helps the host sense invading pathogens and promote an adaptive immune response. The various inflammation pathways are NOD, LRR, and NLRP3 [13]. NLRP3 comprises three separate parts: the pyrin domain is at the N-terminal end, the NACHT domain is in the middle, and the C-terminal domain is full of leucine-rich repeats [14]. The IL-1 β levels led to the rise in NLRP3, and caspase-1 was significantly elevated in the PF model's untreated bronchoalveolar lavage fluid macrophages [15]. When the PF models are induced with the BLM, the level of the NLRP3 was found to increase, which shows that the pathways were majorly involved in inducing PF. The MV can inhibit the NLRP3 pathway, thereby reducing the risk of PF. The level of NLRP3 was high in lung tissue, and it was the major catalyst found in initiating the PF [14]. The NLRP3 inflammasome initiates normal processes such as ion channels, mitochondrial autophagy, excessive ROS production, and lysosome rupture [16]. The MV can also release Pro-inflammatory cytokines, such as IL-1 β , and ROS, that trigger the NLRP3. The NLRP3 inflammasome, a crucial marker of cellular stress, enhances inflammatory responses by activating interleukin-1 β (IL-1 β) and interleukin-18 (IL-18). This inflammasome-driven inflammation aggravates the progressive deterioration of lung damage in fibrotic conditions. The MV's intervention against the oligomers in NLRP3 mitigates the process and reduces lung inflammation. This study indicates that MV confers protective effects by mitigating oxidative stress, diminishing NLRP3 inflammasome activation, and alleviating inflammatory and fibrotic responses in the lungs. The research aims to clarify the mechanisms underlying Malvidin's actions and identify a novel therapeutic approach for PF.

Materials and methods

Reagents

This study utilized DMEM and Ham's F12 media with 5% FBS and streptomycin for cell culture. Growth factors, including bovine pituitary extract, insulin, insulin-like growth factor, transferrin, and EGF, were obtained from Thermo Fisher Scientific (Waltham, USA). Malvidin was purchased from Shanghai Yuanye Bio-Technology (Shanghai, China), while BLM was sourced from Tianjin Taihe Pharmaceutical Limited Corporation (China). The MTT assay kit (3-(4,5-dimethylthiazol-2-yl)-2,5-diphenyltetrazolium bromide) and hematoxylin and eosin (H&E) staining kits were acquired from Beyotime Biotechnology (Shanghai, China). Biochemical assays included LDH, ALP, and Griess reagent. Oxidative stress markers such as SOD, Glutathione (GSH), Catalase (CAT), (Glutathione) GPX, MPO, Malondialdehyde (MDA), and DCF-DA were kits from Jiancheng

Bioengineering Institute (Nanjing, China). Antibodies for iNOS, eNOS (Thermo Fisher, USA), TXNIP, HIF-1 α (Bioassay Technology, China), NLRP3, ASC, IL-1 β (Cell Signaling), and caspase-1 (Santa Cruz) were used. RNA extraction and PCR utilized the PrimeScript RT kit (Takara, Japan) and SYBR Green Master Mix (Yeasen Biotech, China). The antibodies were purchased from Abmart (Shanghai, China). Protein analysis was performed using SDS-PAGE, PVDF membranes (Millipore), chloramine-T, and Ehrlich's reagent purchased from Sigma-Aldrich, St. Louis, USA.

In silico studies

The in-silico analysis was performed to dock samples in a high throughput range using the AutoDock 4.2 simulation. The compound was obtained from Pub Chem (Malvidin (ID:159287)) and sourced the NLRP3 protein structure from the Protein Data Bank (PDB ID: 8ETR). We docked Malvidin against NLRP3 to calculate the binding affinity score. The docking process was initiated by creating the protomol using a ligand-based technique. The protomol threshold to 0.5 and left the bloat at 0 by default for the samples. Rotation and conformation maximum values for docking were 20 and 100, respectively. Superior scores signify improved ligand-receptor docking. We determined the values for the acceptance score and overall score [17].

Cell culture

The BEAS-2B cells, a human bronchial epithelial cell line, were cultured at 37 °C in a condition with 5% CO₂, utilizing DMEM media supplemented with 100 μ g/mL of streptomycin, 100 U/mL of penicillin, and 5% FBS. The RLE-6TN, also known as CRL-2300, is a different rat lung epithelial cell line that was cultured in Ham's F12 medium supplemented with 0.01 mg/mL of bovine pituitary extract, 5ng/mL of insulin, 2.5 ng/mL of insulin-like growth factor, 1.25 μ g/mL of transferrin, 2.5 ng/mL of EGF, and 10% SFB. The study analyzed the PF model in vitro using both cell lines, which were purchased from Shanghai Kanglang Biotechnology Co., Ltd. (Shanghai, China) [18, 19]. The BLM solution was prepared by dissolving in 0.9% of PBS, and the cells were cultured in a medium exposed to BLM (200 μ g/mL) and allowed to be treated for 4 days, and the PBS was used as a control. The BLM-induced cells were treated with various concentrations of MV (50, 100, 150 μ g/mL), and the changes were observed. Group I indicates the control, Group II: BLM-induced model, Group III: BLM + 50 μ g/mL, Group IV: BLM + 100 μ g/mL, and Group V: BLM + 150 μ g/mL.

In vitro analysis

Cell viability assay

The cell viability assay used BEAS-2B and RLE-6TN cell lines. The cells were cultivated in 96-well plates with different concentrations of prepared MV (50, 100, and 150 μ g/mL) and allowed to culture for 24 h. After this, 5.0 mg/mL of MTT dye solution was added, and the cells were incubated for 4 h at 37 °C. The supernatant was discarded and replaced with 150 μ L of dimethyl sulfoxide (DMSO). The absorbance was measured at 490 nm using a microplate reader [20]. The fixed cells were washed with PBS and then they were added with 60 μ g/mL of AO dye and incubated for 3 min. Further these cells were washed in PBS and the changes was observed at 488 nm in a fluorescence microscope.

Measurement of intracellular ROS production

The intracellular ROS was analyzed using the differences between the cell types before and after the treatment. After being arranged in 96-well plates at a density of 2×10^4 cells/well, the BEAS-2B and RLE-6TN cell lines were allowed to grow for an entire day. The BLM-induced cells were exposed to the MV at various concentrations (50, 100, and 150 μ g/mL). The cells were incubated with 2',7'-dichlorofluorescein diacetate (5 μ M of DCF-DA) for 30 min at 37 °C in a dark environment. Further, the cells were washed with PBS and the fluorescence changes were observed with a fluorescence microscope [21].

Wound scratch assay

The migration of fibroblasts was evaluated using a wound scratch experiment. The BEAS-2B and RLE-6TN cells were grown and inoculated in a 6-well plate at a density of 2×10^5 . The cells were grown until they reached 90% confluent. Then, the scratches were made using 200 μ L sterile pipette tips. After incubating the cells with BLM and subsequently treating them with MV at various concentrations (50, 100, and 150 μ g/mL), changes were assessed at 0, 24, and 48 h to measure the pace of wound healing. Images of the plates were obtained at various time intervals using a microscope (Sanshen, Shanghai, China). The relevant regions of the wounds were analyzed with ImageJ software to measure and determine the cell scratch area [22].

In vivo analysis

Both male and female C57BL/6 mice, aged 6–8 weeks and weighing approximately 20–25 g, were obtained from the Shanghai Animal Center in China for in vivo analysis. The animals were kept in a 12-hour light-dark cycle with food and water provided. The animal ethical committee approved the mice-related procedures under Approval No. A2023NSFSC1730. The PF was induced by intraperitoneal injection of ketamine (75 mg/kg) and xylazine

(5 mg/kg), and bleomycin (3 mg/kg, in 0.9% saline) was instilled intratracheally [23].

Experimental design

For the analysis of PF, the mice were randomly divided into five groups, with 5 animals in each group: group 1 received saline, group 2 received BLM, group 3 received BLM with MV at 5 mg/kg, group 4 received BLM with MV at 10 mg/kg, and group 5 received BLM with MV at 15 mg/kg [24]. Initially, on day 0, the mice were injected with saline, and the BLM dissolved in saline was injected on frequent days until day 28. They were given MV once daily from the day of BLM treatment by intraperitoneal [17]. After the treatment, the mice were euthanized, by carotid exsanguination just after loss of consciousness by sodium pentobarbital (2.21 ± 0.35 min. for 50 mg/kg and 1.1 ± 0.24 min. for 100 & 150 mg/kg) [25]. Lung tissue was processed for histopathological examination (H&E and Masson's Trichrome staining), hydroxyproline (HYP) content measurement, oxidative stress markers (MDA, MPO, GSH, SOD, CAT), and inflammation markers (NLRP3, TXNIP). Throughout the experiment, the body weight of the mice was measured weekly to monitor changes. Upon completion of the study, the mice were anesthetized, and the entire lung was extracted, rinsed in a saline solution, and weighed. The lung index was determined by dividing the wet lung weight (mg) by the body weight (g).

Sample collection

Blood specimens were collected from the tail vein. A topical anesthetic cream must be applied on the tail's surface 30 min before the experiment. A 23G needle is introduced into the blood artery to collect blood using a capillary tube or a syringe with a needle. Blood was collected in centrifuge tubes and subjected to centrifugation at 3000 rpm for 20 min. The lungs and bronchoalveolar lavage fluid (BALF) of the mice were promptly excised and subsequently partitioned into two segments [26]. Part of each organ was immediately placed in 10% (v/v) formal saline for histological examination and the rest was kept at -80°C for subsequent assays. The lungs were homogenized (10% w/v) in ice-cold 0.1 M Tris-HCl buffer (pH 7.4). The homogenate was centrifuged at 3000 rpm for 15 min at 4°C and the resultant supernatant was used for biochemical analysis. The trachea was exposed, cannulated, and secured with suture thread, followed by 3 in-and-out washes using 0.6 mL of isotonic saline solution. The efficacy of BALF collection varied between 50 and 100% of the total solution administered. The BALF was centrifuged at 1500 rpm for 15 min at 4°C , and the resulting pellets were collected for cell counting. Supernatants were separated and maintained properly for later biochemical investigations [27].

BALF analysis

A tracheal tube was inserted into the trachea to collect the BALF, and these cells were resuspended and used for counting inflammatory cells [28].

Evaluation of antioxidant biomarkers and oxidative stress in lung homogenates

MDA in lung tissues was believed to be a marker of lipid peroxidation, where lung tissue homogenate was used to estimate the MDA content [29]. From the MDA standard curve, the MDA content (nmol/gm) was extrapolated for each sample. The capacity of the SOD enzyme to prevent autoxidation was assessed through SOD activity. Reduced GSH was analyzed using Ellman's reagent. Where CAT and GPX were analyzed using a kit. The assay for each sample was determined using a standard curve, following the manufacturer's instructions. A key indicator for pulmonary fibrosis assessment is tissue myeloperoxidase (MPO), an enzyme involved in oxidative stress and inflammatory cascades. Changes in MPO levels were measured using an ELISA kit after homogenizing the lung tissue [30].

Assessment of serum markers

The lactate dehydrogenase (LDH) and alkaline phosphate (ALP) serum levels were measured using the manufacturer's instructions. The auto-hematology analyzer (Diagon Ltd. D-cell 60, Hungary) was used to measure the number of sedimented cell pellets. The experiment was conducted, and the absorbance was measured at 598 nm [31].

Assessment of NOx, eNOS and iNOS protein expression

The NOx level was assessed using nitrate reduction by vanadium (III) combined with an acidic Griess reagent, allowing for the determination of total nitrite/nitrate content. The absorbance was recorded at 540 nm, and the NOx concentration was interpolated for each sample according to the predefined curve. The iNOS and eNOS antibodies were procured from Thermo Fisher Scientific (Kalamazoo, MI, USA). According to the manufacturer's guidelines, the experiments were conducted with HE staining with a mouse polyclonal antibody at a 1:20 dilution and a mouse monoclonal antibody at a 1:50 dilution. The staining intensity of each specimen for a specific antigen was assessed on a semi-quantitative scale ranging from 0 to 3, where 0 indicates no expression, 1 signifies weak expression, 2 represents moderate expression, and 3 denotes strong expression [32].

Hydroxyproline (HYP) analysis

This analysis was used to determine the degree of collagen deposition, and HYP content was determined by the colorimetric method. The lung tissue was exposed to an

alkaline solution instead of an acidic pH that would cause tissue degeneration. The lung samples were incubated at 37 °C for one night with 5% KOH, followed by a hydrolysis step using 10 N NaOH and a 3 h incubation period with chloramine-T solution. Ehrlich's reagent treated the sample and kept it in the water bath at 65 °C for 20 min to form a chromophore detectable at a wavelength of 550 nm using a colorimeter WPA color wave (Cambridge, UK) [33].

Assessment of TXNIP and HIF1 α contents

By the manufacturer's guidelines (Bioassay Technology Laboratory Company, Shanghai, China), the thioredoxin interaction protein (TXNIP) and HIF1 α were assessed in both lung homogenates and bronchoalveolar lavage fluid (BALF) using an ELISA kit.

Histopathological examination for lung tissue

The preserved animal's lungs were immersed in 10% formalin, thereafter embedded in paraffin, and sectioned with a microtome. Conducted a comprehensive assessment of lung damage and fibrosis by staining tissue sections with H&E dye and Masson's Trichrome to evaluate the extent of injury. Tissue slices were examined under a light microscope for inflammation, bleeding, and fibrosis. The grading system for alveolitis and fibrosis was assessed on a scale from 0 to 3, where a score of 0 indicates no alveolitis/fibrosis, 1 signifies mild distribution, 2 denotes moderate distribution, and 3 represents severe distribution [28].

Real-time quantitative PCR

The total RNA was extracted from the lung tissue as per the manufacturer's instructions. Using the PrimeScript RT reagent kit with gDNA Eraser (Takara, Shiga, Japan), reverse-transcribed into first-strand cDNA. The SYBR Green Master Mix Kit (Yeasen Biotech Co., Ltd., Shanghai, China) was used for real-time PCR analysis to determine the mRNA levels of collagen 1, IL-1 β , fibronectin, α -SMA, NLRP3, ASC, and caspase 1. The Q-PCR conditions were: 95 °C for 2 min, followed by 40 cycles of 95 °C for 3 s and 60 °C for 30 s, with a melting curve of 60–95 °C. The primer sequences used in this experiment are listed in Supplementary File 1. GAPDH was used as an internal control. Relative mRNA expression levels were quantified with $2^{-\Delta\Delta C_t}$ method. Primers used for RT-qPCR were synthesized by Sangon Biotech Co., Ltd [20].

Western blotting analysis

The electrophoresed protein samples from fibroblasts and lung tissues on 12% sodium dodecyl sulfate-polyacrylamide (SDS-PAGE) gels and then transferred onto PVDF (polyvinylidene fluoride) membranes from

Millipore. Then, the membranes were incubated with primary antibodies NLRP3 (1:1000, Cell Signaling Technology), ASC (1:1000, Cell Signaling Technology), β -Tubulin (1:1000, Cell Signaling Technology), were all measured overnight at 4 °C. Then, the secondary antibodies were added and incubated in the membranes for 1.5 h at 37 °C. A Bio-Rad ChemiDOC TM MP Imaging System was employed to acquire the images [21].

Statistical analysis

Data were analyzed using GraphPad PRISM software (version 6.0; San Diego, CA, USA) and are expressed as the mean \pm standard deviation (SD). One-way analysis of variance (ANOVA) was employed to assess differences among various groups, proceeded by the Bonferroni post hoc test for pairwise comparisons. $P < 0.05$ was considered statistically significant.

Results and discussion

In silico analysis

During the docking analysis, the binding sites of the protein molecule and the ligand are indicators to determine their interaction. The lowest binding affinity indicates the most significant match for bioactive compounds. In this study, the compound MV was docked against NLRP3, which was found to have a binding affinity of -7 Kcal/mol. The NLRP3 (PDB ID: 8ETR) was found to have a resolution of 3.50 Å, and they were analyzed by electron microscopy. The compound MV has better interaction with NLRP3, which includes residues GLY A:231, GLY A:229, ALA A:228, ILE A:230, LYS A:232, HIS A:522, THR A:233, MG A:701, LEU A:413, ILE A:234, MET A:523, TRP A:416, PRO A:412, LEU A:171, TYR A:381, PHE A:373, ARG A:167, THR A:169, ARG A:167, TYR A:168. 2 pi-cations, 9 van der Waals, 6 conventional hydrogen bonds, an alkyl, and pi-alkyl were obtained, as shown in Fig. 1. This suggests that a higher binding affinity can inhibit NLRP3 pathways, thereby reducing fibrosis. This analysis has selected the compound MV for further in vivo and in vitro testing. The literature revealed that NLRP9 more effectively docks with *Withania somnifera* to treat inflammation. In the process of developing the drug, the molecular docking method revealed structure deviation, protein compactness, stability, mobility, and hydrophobicity. These factors were essential in the drug's development. Furthermore, they showcase the potent and efficient compounds that have the potential to interact with inflammatory proteins, thereby reducing lung inflammation. Molecular docking was one of the major methods for choosing the drug for the particular treatment that may reduce the risk of side effects and portray the drug's mechanism of action for a better understanding of the process [34, 35].

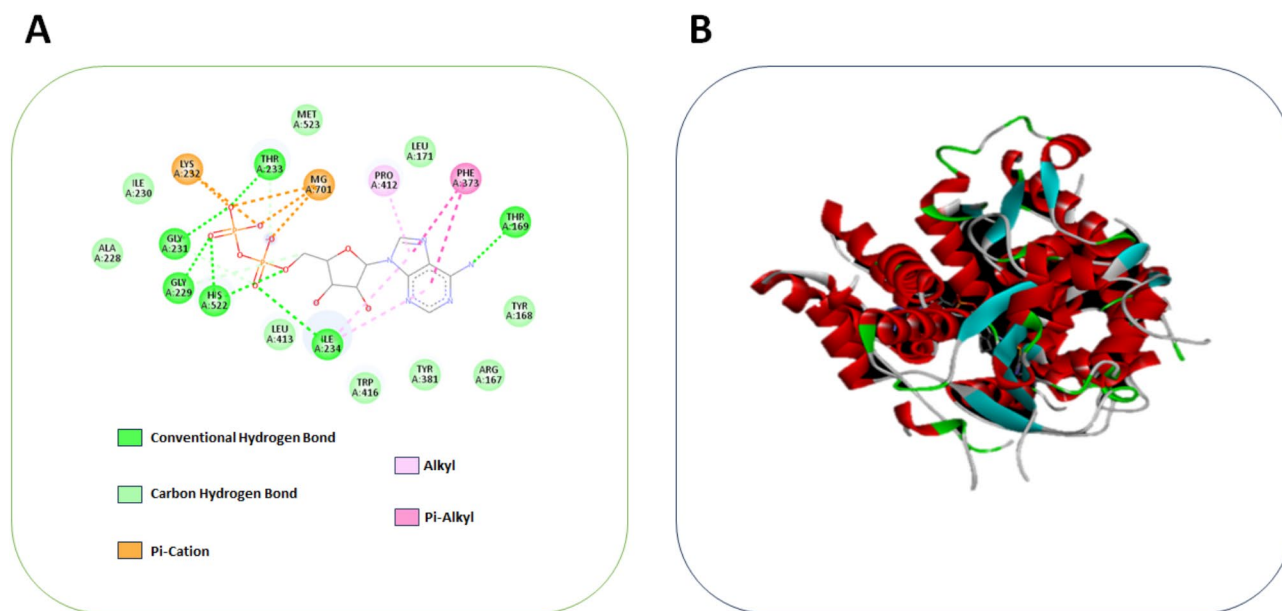


Fig. 1 **A** Computational model illustrated docking of compound Malvidin against NLRP3 and **B** Denotes the 3D structure of MV binding to NLRP3

In vitro analysis

The in vitro analysis was used in the fields of pharmacology, toxicology, molecular biology, and genetics. They provide the molecular and cellular mechanisms, which might be difficult to observe in vivo. From the supplementary Fig. 1(A&B), the effect of MV on BEAS-2B and RLE-6TN was observed up to the concentration of 250 $\mu\text{g}/\text{mL}$. From that, it was observed that the IC_{50} was found to be at 100 $\mu\text{g}/\text{mL}$. So, further analysis was carried out at the concentration of 50, 100, 150 $\mu\text{g}/\text{mL}$. After this optimization, the MTT assay was carried out on BEAS-2B and RLE-6TN, induced with BLM, which were treated with different concentrations of MV (50, 100, and 150 $\mu\text{g}/\text{mL}$), and the cell viability was examined. Figure 2A illustrates the fluorescence changes of BEAS-2B and RLE-6TN cell lines at different treatment levels, demonstrating the effective cell proliferation by AO staining analysis. The BLM induced group shows less fluorescence when compared to the treated group. This proves that MV was efficiency in treating PF. Figure 2B shows that cell viability was reduced when treated with BLM; in contrast, when treated with the MV, the cell viability increased, which shows that the MV was effective in treating the PF. The BEAS-2B shows significance of $p < 0.001$ for the treated and induced group and has $p < 0.05$ for the treated group, the RLE-6TN was also found to have a similar significance. Hence, this MTT was used to prove the biocompatibility of the MV in mitigating PF. The MTT significantly reduces fibroblast proliferation and metabolic activity, showing that MV has potential as an anti-fibrotic agent. Malvidin's antioxidant properties likely played a pivotal role in scavenging ROS and reducing oxidative stress, thereby mitigating cellular

damage. Furthermore, the reduction in oxidative stress may have indirectly suppressed the activation of the NLRP3 inflammasome, a key mediator in BLM-induced fibrosis [36, 37]. One of the pathophysiological features of lung function failure (PF) is the excessive buildup of extracellular matrix elements like collagen, which causes the scarring and stiffening of the lung tissue. ROS plays a significant role in this process. Increased ROS levels can trigger fibrotic pathways through cellular damage and oxidative stress. Therefore, research has demonstrated that ROS enhances the inflammatory response by elevating PF and triggering the release of inflammatory cytokines. This implies that BLM is crucial in controlling ROS production and maintaining genomic stability during cell damage. Increased ROS production, persistent inflammation, and DNA damage brought on by BLM induction all contribute to the development of fibrosis [38, 39]. Figure 2C shows that the induction of BLM into the cell lines led to an increase in ROS levels. Conversely, when the cell lines were treated with MV, the ROS levels decreased, suggesting that the cells can regulate the oxidative damage caused by BLM. Figure 2D displays the graphical changes in the ROS level for both cell lines, which proves that the MV was effective in mitigating PF, and observed that the BEAS-2B was found to have the significance of $p < 0.001$ for the induced and control group and $p < 0.05$ for the induced and treated group. The cell RLE-6TN has the significance of $p < 0.001$ for the induced and control group and $p < 0.05$ for the induced and treated group. Malvidin and its glycosides, along with the anthocyanins in blueberries, can substantially reduce ROS levels in endothelial cells and alleviate detrimental effects by modifying the concentrations of certain critical proteins. The

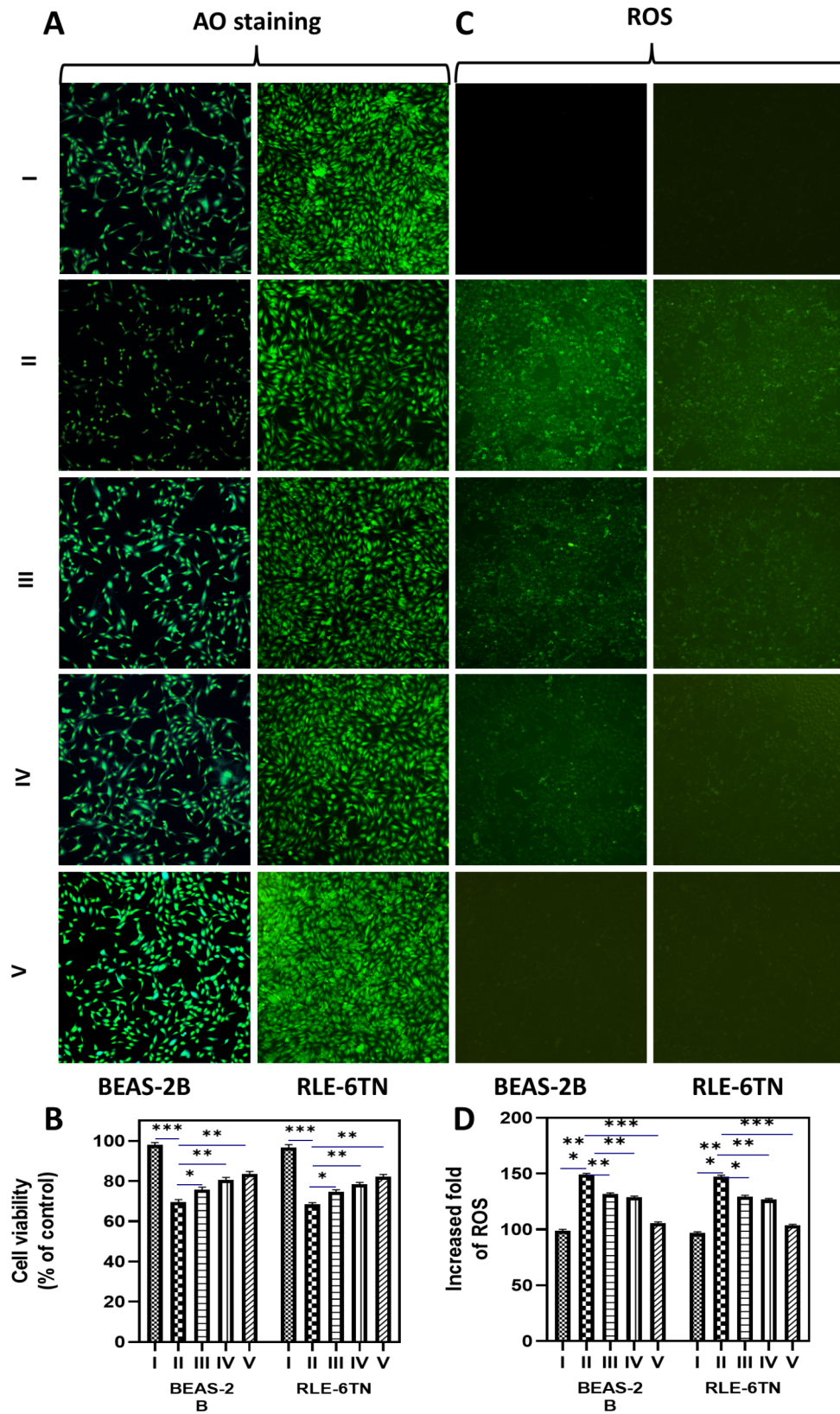


Fig. 2 **A** Fluorescence image of BEAS-2B and RLE-6TN to determine the cell viability using AO staining, where, **B** The graphical analysis of cell viability where, Group I represents control, Group II for the BLM-induced group, Group III for BLM+ MV (50 µg/mL), Group IV for BLM+MV (100 µg/mL), and Group V for BLM+MV (150 µg/mL), **C** Indicates the fluorescence changes of ROS in both the cell lines and **D** Denotes the graphical changes of ROS. Data are expressed as mean ± standard deviation, sample size (n) = 3 for each group, *P < 0.05; **P < 0.01; ***P < 0.001

ROS is crucial in activating the NLRP3 inflammasome, a multiprotein complex associated with inflammation and fibrosis. Increased ROS levels work as an essential signal for NLRP3 activation, resulting in the cleavage pro-caspase-1 into its active form and the subsequent release of pro-inflammatory cytokines, including IL-1 β and IL-18. The NLRP3 inflammasome is crucial in forming and progressing pulmonary fibrosis by regulating inflammatory responses, activating fibroblasts, and altering the extracellular matrix. Targeting the NLRP3 inflammasome and its subsequent effects presents a viable method for the treatment of PF [40, 41]. The wound area was analyzed using the wound-healing assay, and observed changes in cell movement at different time intervals between 0, 24, and 48 h, as shown in Fig. 3(A&B). The BLM-induced BEAS-2B and RLE-6TN cell lines have less wound recovery when treated with the MV; it has a high migration rate. Figure 3C represents the graphical representation of wound recovery; it was found to have a significance of $p < 0.001$ for the control and the induced group. The $p < 0.05$ for the induced and treated group. Inflammatory cells and pathways can directly harm lung tissue by producing elastases, cytokines, and growth factors that encourage fibrosis. This process led to fibrotic alterations and disruptions to wound-healing mechanisms. Hence, wound healing was a major factor in analyzing the PF. The in vitro analysis confirms the synthesized MV was safe and effective in mitigating PF. Further, the MV was taken to the in vivo analysis to determine the efficiency of MV in alleviating PF. Figure 3D represents the schematic representation of the wound healing assay.

In vivo analysis

Mice were utilized in the analysis; the BLM induced mice were treated with MV. The BLM plays a major role in PF; they are extensively used to test anti-fibrotic, anti-inflammatory, and antioxidant therapies. BLM is relatively inexpensive and easy to administer, providing consistent and reproducible results in animal models. They were further treated with MV and the changes have been monitored. Figure 4A represents the schematic representation of the in vivo analysis. Figure 4B shows the alterations in weight seen in mice subjected to MV therapy at various doses and those undergoing BLM-induced treatment. The BLM-induced mice model was utilized to determine the anti-fibrotic mechanism. It was observed that $p < 0.001$ for the treated and induced group. From this, it was observed that BLM causes significant weight loss, and when treated with MV, that significantly enhances the weight gain. Figure 4C shows the analysis of lung-wet-to-dry ratio, which was high for the induced mice model, and it was found to be decreased for the treated group with the significance of $p < 0.05$. Figure 4D illustrates the effect of MV on the BLM group, resulting in a significant

reduction in the lung index on day 28 compared to the BLM-induced group, and it was found to have $p < 0.05$ when compared to the treated group.

Figure 4(E-H) indicates that the compound went through an analysis of BALF, revealing that the BLM-induced model exhibited elevated leukocyte levels with a significance of $p < 0.001$ in BALF. Treatment with MV reduces the total leukocyte count, affecting neutrophils, lymphocytes, and increasing the macrophage level. BLM therapy increases the typical proportions of neutrophils and lymphocytes and markedly lowers macrophage levels ($P < 0.05$). The macrophage level decreased in the BLM-induced model; however, treatment with the MV led to an increase, demonstrating the drug's efficacy in alleviating PF. The MV has an antioxidant capacity, an anti-inflammatory effect, and a potential effect on PF. MV may inhibit fibroblast proliferation and differentiation, reducing the excessive deposition of ECM; hence, it has been proven effective in mitigating PF. MV treatment significantly reduced these fibrotic markers like decreased collagen deposition, inhibition of fibroblast activation (α -SMA), and downregulation of fibrotic mediators (TGF- β) [40, 42]. Figure 4J schematic representation of the changes in the body weight of the mice.

Examination of antioxidant and oxidative stress biomarkers in lung homogenates

The BLM-induced PF mice model and the normal control mice have different levels of MDA, SOD, GSH, MPO, and antioxidant activities of GPx and CAT. Figure 5 (A-F) demonstrated that BLM induced higher levels of MDA and MPO with a significance of $p < 0.001$. Following MV treatment, there was a decrease in MDA and MPO levels ($p < 0.05$) between the induced and treated groups, suggesting a reduction in oxidative stress. This shows that BLM administration causes increased oxidative stress, which damages cells. When they received MV treatment following the BLM injection, the levels of SOD, GSH, CAT, and GPx in the lung tissue significantly decreased with the significance of $p < 0.001$. It was demonstrated that the MV treatment led to the upregulation ($p < 0.05$) of these antioxidant factors and prevented the decline in antioxidant enzyme activities to levels comparable to the control group. The graph revealed that MDA serves as an assay for lipid peroxidation. Compared to the healthy control group, the lung tissues of the BLM-induced mice model had higher levels of MDA, which suggests that ROS was damaging the lungs. The decrease in MDA levels indicates a significant and dose-dependent scavenging of ROS by MV at doses of 5, 10, and 15 mg/kg. The imbalance between high ROS and low antioxidant defense, which results in oxidative stress and recognized molecular initiating events, essentially causes PF [43]. Among these, NADPH, NOXs, MPO, and EMT were thought to

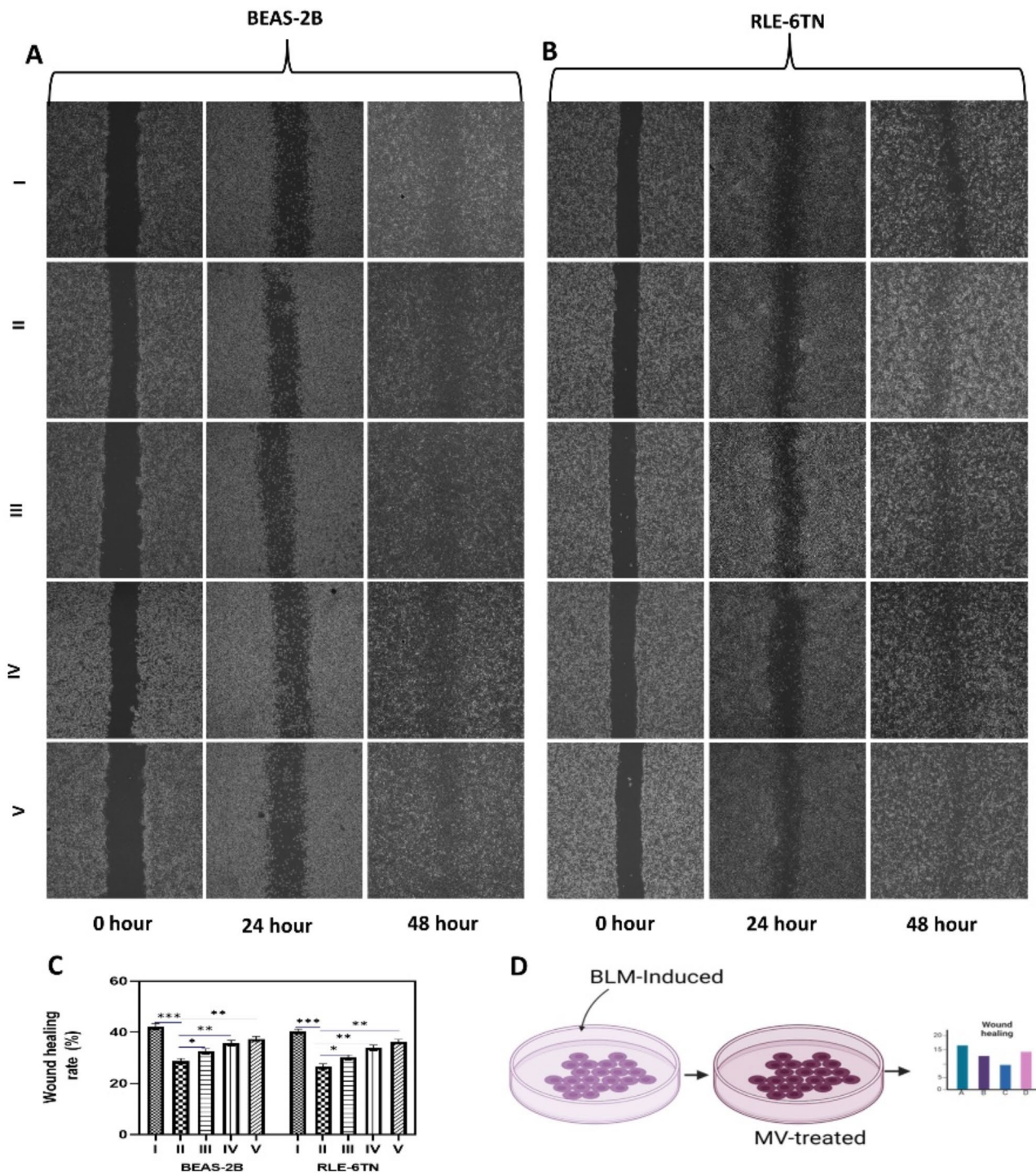


Fig. 3 **A & B** Indicates the wound scratch assay at various time intervals of 0 h, 24 h, and 48 h and this shows that wound healing was high when treated with MV on both BEAS-2B and RLE-6TN cell lines the images were at 4x magnification, **C** Graphical representation of wound healing rate at percentage, **D** The schematic representation of the wound healing activity in BLM-induced cell lines. Data are expressed as mean ± standard deviation, sample size (n) = 3 for each group, **P* < 0.05; ***P* < 0.01; ****P* < 0.001

be the main producers of ROS, which can trigger fibrogenesis in myofibroblasts and the inflammatory response. Low molecular weight endogenous antioxidant enzymes (SOD, CAT, GHx) that can boost endogenous antioxidant

enzyme synthesis or remove reactive species are being suggested and developed as possible treatments for PF [44]. Antioxidant enzymes reinforce the body’s defence system against ROS. SOD can convert $O^{•2-}$ into H_2O_2 ,

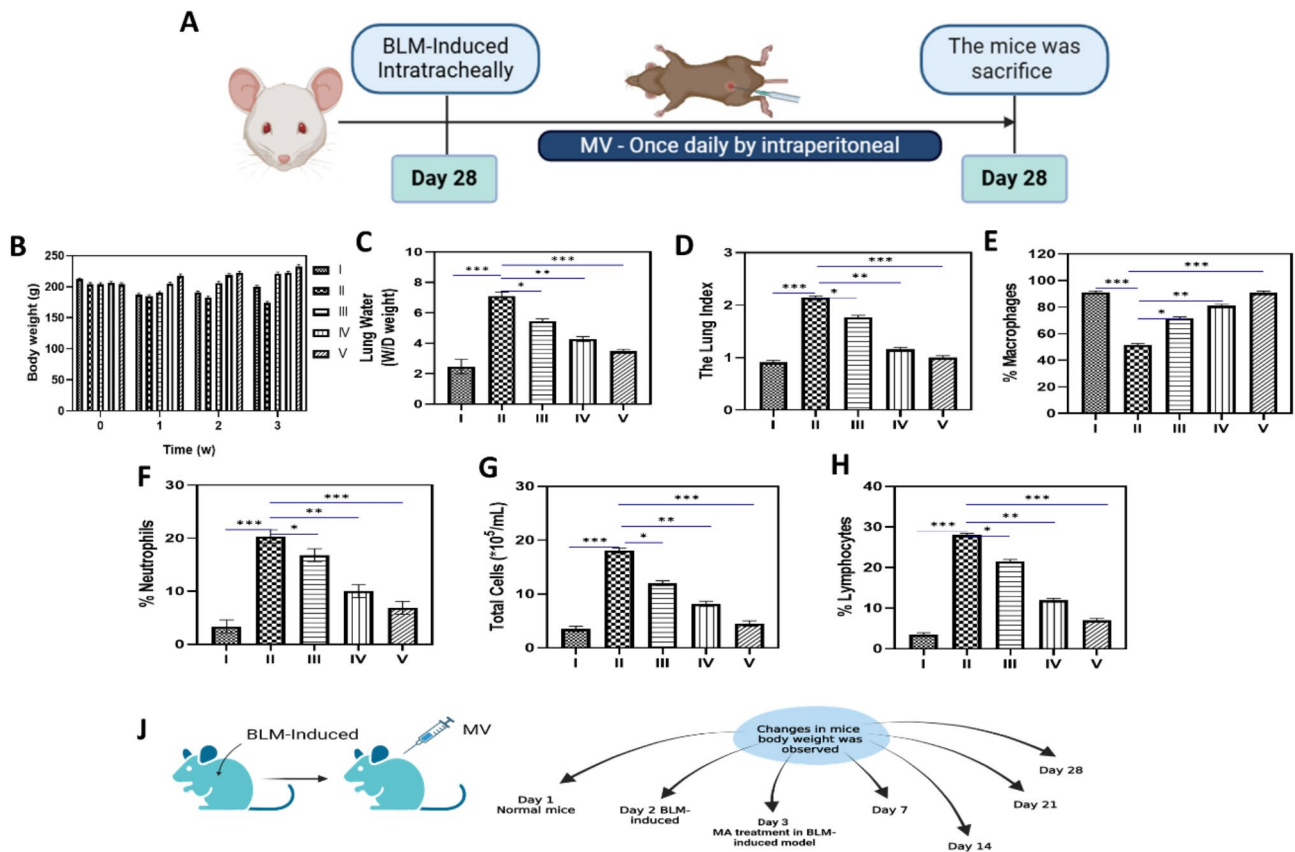


Fig. 4 **A** Schematic representation of BLM-induced mice model treated with MV, **B** Denotes the changes in the body weight of the BLM-induced mice treated with MV, **C** Lung wet to dry weight ratio analysis, **D** Effect of Lung index, where (**E-H**) indicates the percentage of Macrophages, Neutrophils, Total cells, and Lymphocytes changes in BALF analysis, **J** Shows the schematic representation of observation of the body weight changes in BLM-induced mice treated with MV. Data are expressed as mean \pm standard deviation, sample size (n) = 3 for each group, * $P < 0.05$; ** $P < 0.01$; *** $P < 0.001$

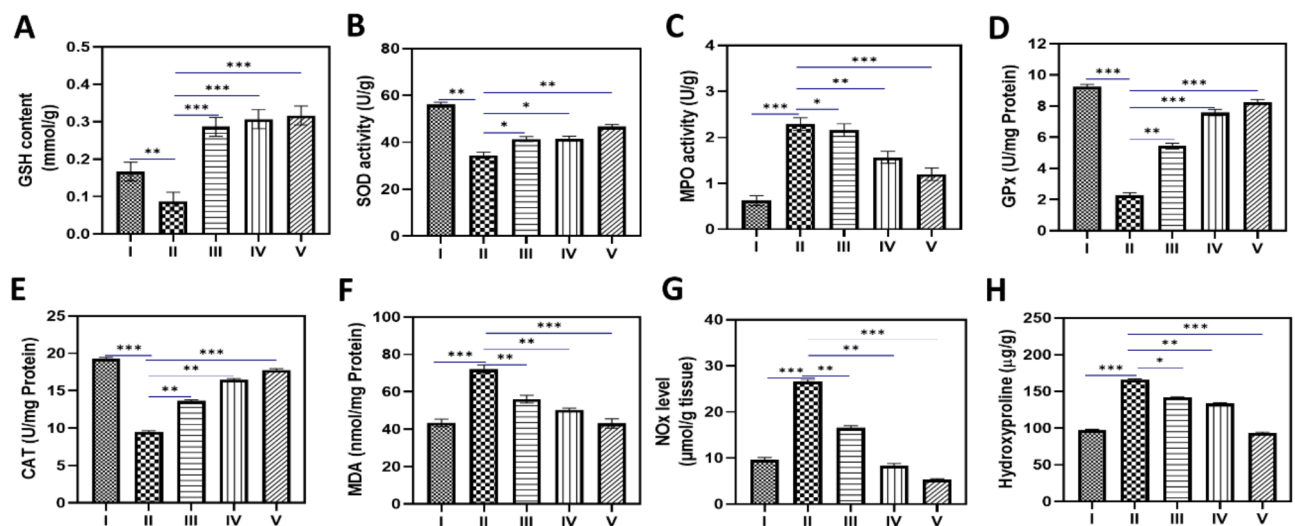


Fig. 5 **A-F** The impact of administration of MV on oxidative stress and antioxidant biomarkers in lung homogenates of BLM in mice and found that MDA and MPO were found to be high in BLM-induced model when treated with MV the activity has been reduced, **G** NOx level which also plays the major role in PF and **H** indicates the HYP content the activity was significantly decreased for BLM-induced and treated group. Data are expressed as mean \pm standard deviation, sample size (n) = 3 for each group, * $P < 0.05$; ** $P < 0.01$; *** $P < 0.001$

which is then catalysed by GSH-PX and CAT to produce H_2O and O_2 . The upregulation of these genes leads to a heightened capacity of cells to withstand the effects of oxidative stress, external agents, and electrophilic compound stimuli. The decrease in antioxidant enzyme activities, such as SOD and CAT, along with an increase in NLRP3 expression prevents PF [45]. Figure 5G shows the NOx level also tends to increase in the BLM-induced model ($p < 0.001$). When treated with MV, the level tends to reduce significantly ($p < 0.05$), indicating the reduction in oxidation stress and inflammation, such as physiological and pathological processes, and that NO plays various roles in PF. NO is a signaling molecule and the amounts of nitrite and nitrate in biological fluids and tissues can reveal information about the degree of oxidative stress and NO production, which are linked to PF [39]. MV treatment significantly reduced the BLM-induced changes in lung iNOS and eNOS expressions within the BLM-induced cohort. These outcomes were attained by reducing iNOS and elevating eNOS protein, which reverted to nearly normal levels. The BLM-induced group has significantly elevated iNOS protein expression and a decrease in eNOS protein expression. The primary factor contributing to lung function failure was the synthesis of nitric oxide (NO), mediated by three isoforms of nitric oxide synthase: nNOS, located in neurons; eNOS, the constitutive endothelial type with protective vasodilatory effects; and iNOS, activated by inflammatory cells and responsible for stimulating cytokine-activated macrophages within the alveoli [40]. The constriction of the lumen of the lung artery causes a reduction of eNOS levels; however, in response to the invasion of inflammatory cells, the iNOS protein levels were increased [41].

The lung HYP was the major factor known as a biomarker of PF. From Fig. 5H, it was observed that the level of HYP was increased when the mice were induced with the BLM ($p < 0.001$), and when treated with the MV ($p < 0.05$), the level was reduced. As a result, measuring hydroxyproline levels provides an accurate assessment of collagen deposition and the severity of fibrosis. It is essential to comprehend the etiology of PF and assess the effectiveness of treatment approaches. By focusing on collagen synthesis and deposition, which improve lung function, the potential therapies are to lower hydroxyproline levels and lessen fibrotic changes. HYP, a significant marker of the amount of collagen in lung tissue, is commonly measured to determine the degree of fibrosis [42]. Figure 6A shows the mortality rate of the mice before and after the treatment when the BLM was induced in the mice model, which causes cell damage and leads to the death of the animal. When the BLM-induced group was treated with the MV, survival increased, which confirms the potential of MV in mitigating PF. Figure 6(B-E) shows that MV significantly reduces the overall protein concentration in the BALF of mice induced with BLM. Serum ALP, LDH, and BALF's LDH activity were significantly ($p < 0.001$) higher in mice induced with BLM (group II); MV treatment further confirmed these levels by reducing the activity with a significance of ($p < 0.05$). BLM-induced lung injury is indicated by elevated levels of ALP and LDH, and elevated BALF-LDH activities, which indicate the degree of alveolar damage [46]. BLM instillation also resulted in a marked increase in leukocytic infiltration in peri-bronchiolar tissue, alveolar walls, and it obliterated the alveolar lumen, in addition to a marked increase in airway, vascular, and parenchymal inflammation. In terms of lung inflammation overall and

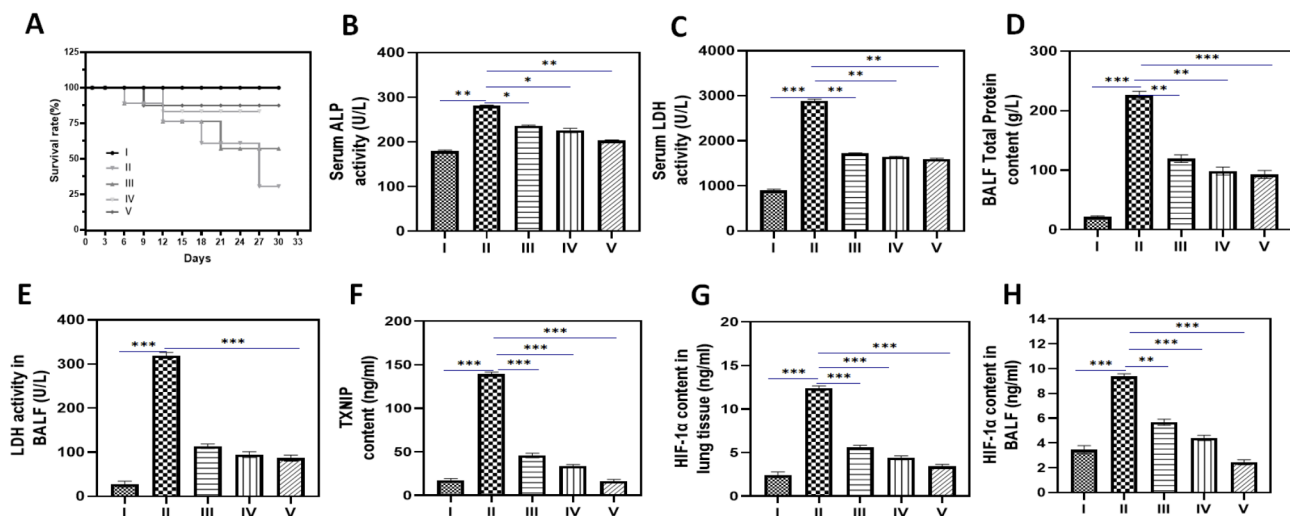


Fig. 6 A Denotes the survival rate of BLM-induced mice treated with MV, where (B-E) Indicates Serum ALP, Serum LDH, BALF total protein, and LDH activity in BALF, and F-H Represents the TXNIP and HIF-1 α level in lung tissue and BALF. Data are expressed as mean \pm standard deviation, sample size (n) = 3 for each group, * $P < 0.05$; ** $P < 0.01$; *** $P < 0.001$

alveolar wall thickness, BLM mice showed significantly higher scores than control mice [31]. After receiving MV at various concentrations, they showed a reduction in inflammation, proving the compound's effectiveness in mitigating PF. Previous studies have demonstrated that MV may lower these inflammation gene transcription levels [47]. Figure 6(F-H) shows that the TXNIP content was measured from the lung tissue homogenate and observed as high for the BLM-induced mice model ($p < 0.001$) when compared to the control group. When they were treated with the MV ($p < 0.05$), the reduction of TXNIP in the lung tissue homogenate and the BALF content level was observed. The MV significantly reduces the lung HIF α ($p < 0.05$) compared to the BLM group. The TXNIP inhibiting NLRP3 inflammasome pathway could help reduce chronic inflammation and its contribution to fibrosis. Targeting TXNIP and its associated pathways offers promising therapeutic potential for mitigating pulmonary fibrosis. However, further research is needed to

understand the mechanisms of TXNIP in fibrosis and to develop effective and safe TXNIP-targeted therapies [29].

Histopathological analysis

The histological examination depicts that the lungs treated with BLM cause damage with obvious lesions, cell infiltration, and tissue decomposition. The changes were analyzed by H&E staining, as shown in Fig. 7A, and found that the BLM-induced model exhibited a higher score when compared to the MV-treated group, with a significance of ($p < 0.05$). Figure 7B shows the MT staining, which was also the other methodology used for the confirmation of PF, which shows the level of the fibrosis and deposition of the collagen. The maximum collagen depositions occurred in BLM-induced mice model when they were treated with MV; the deposition level was reduced, hence, the compound was effectively mitigated PF ($p < 0.05$). Figure 7(C-D) indicates that the histological score, fibrosis score, and Ashcroft score were high in the BLM-induced model when treated with MV; the score

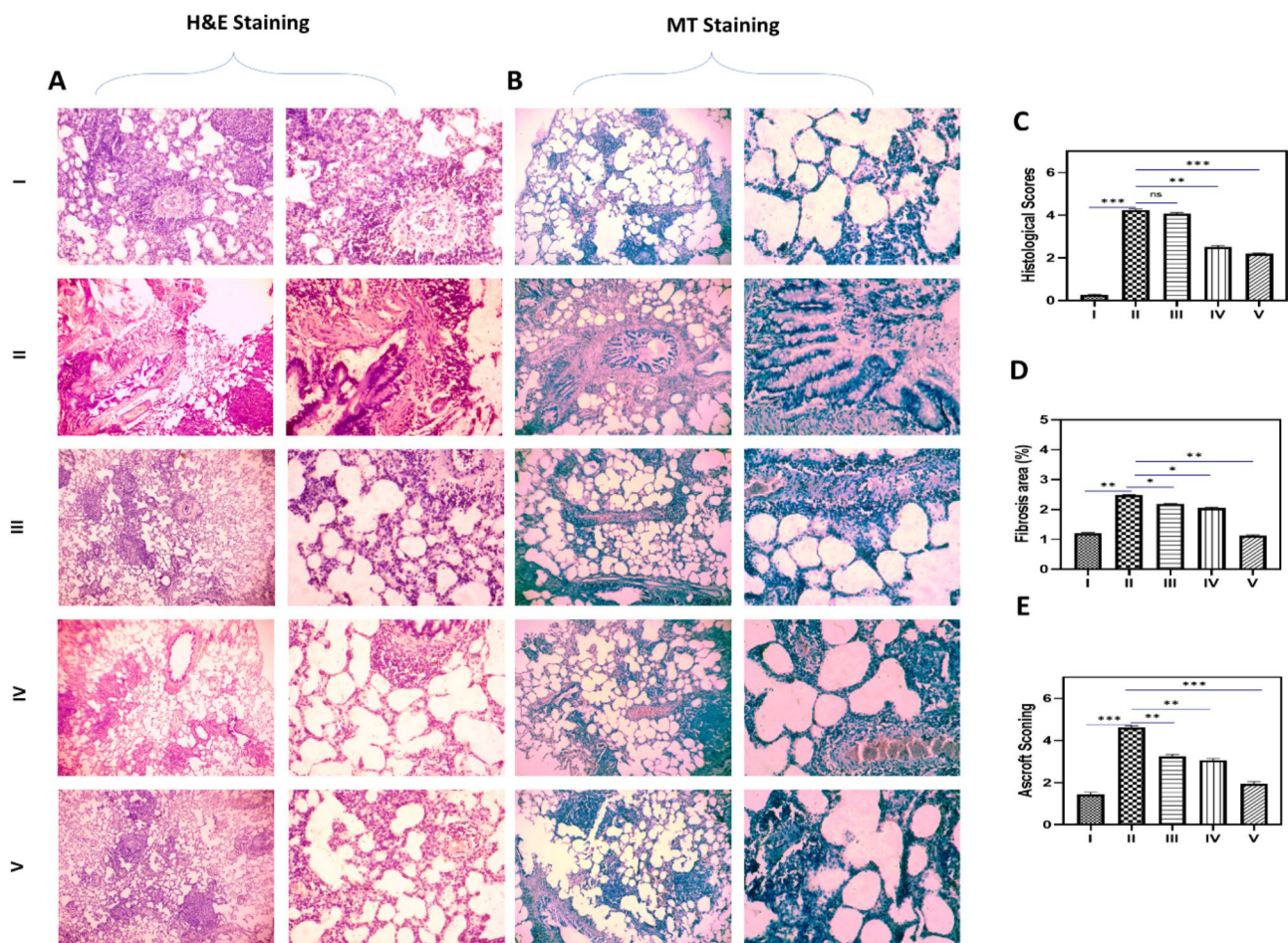


Fig. 7 **A** Displays the damage in mice lung tissue and was determined by H&E staining, **B** Indicates the changes of lung tissue by MT staining, the images were at (20X & 40X). **C** & **D** Graphical representation of the histological score, Denotes the fibrosis area percentage and, **E** Ashcroft's scoring. Data are expressed as mean \pm standard deviation, sample size (n)=3 for each group, * $P < 0.05$; ** $P < 0.01$; *** $P < 0.001$

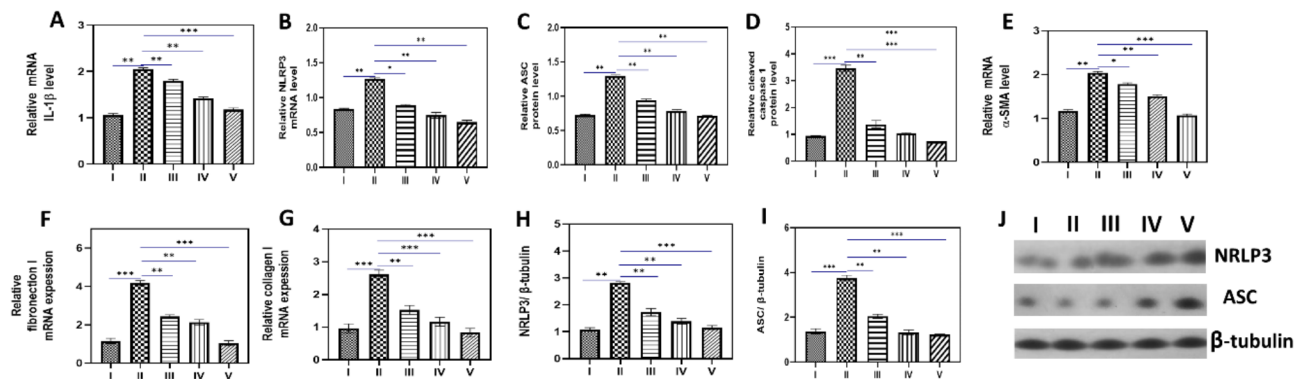


Fig. 8 A-G Represents the qRT-PCR to analyze the expression of anti-inflammatory and anti-fibrotic genes whereas H-I Graphical representation of western blotting changes in NLRP3 and ASC gene and J Western blotting images of NLRP3, ASC. Data are expressed as mean \pm standard deviation, sample size (n) = 3 for each group, * $P < 0.05$; ** $P < 0.01$; *** $P < 0.001$

was reduced, and hence this proves that the fibrosis level has been reduced. The MV has better activity against reducing PF. The preservation of endogenous reserves and inhibition of lipid peroxidation might also support the structural integrity of the basement membrane. Histopathological analysis confirmed the previously mentioned results [48]. MV is a potentially effective treatment option for PF because it combines anti-inflammatory, anti-fibrotic, and antioxidant properties. Furthermore, its natural origin and inclusion in common dietary sources support its favourable safety profile, and the histopathological scores confirm this analysis.

qRT-PCR and Western blotting analysis

NLRP3 activation regulated the induction of BLM-induced inflammatory response. In Fig. 8(A-G), IL-1 β controls the signal cascade producing proinflammatory cytokines ($p < 0.001$) for the BLM-induced and treated group. The mRNA levels of NLRP3, ASC, and Caspase-1, as well as the protein level of NLRP3, increase in the BLM-induced mice model ($p < 0.001$). When treated with MV, the level has been reduced with a significance of ($p < 0.05$). The α -SMA, fibronectin, and collagen play significant roles in pulmonary inflammation, particularly in processes that lead to tissue remodeling and fibrosis, such as in PF. α -SMA marks the activation of myofibroblasts, which contract and deposit ECM. Fibronectin mediates cell adhesion and migration, playing a role in both inflammation and fibrosis. A primary structural protein, collagen accumulates excessively during fibrosis, leading to lung tissue stiffening and scarring. Hence, the level tended to be increased in the induced model when treated with MV, which has been reduced ($P < 0.05$), showing the effectiveness of MV in reducing PF. Following MV treatment, the level dropped, suggesting a reduction in inflammation associated with blocking the IL-1 β signaling pathway and the NLRP3 inflammasome. Hence, the MV compound was better in treating the lung

inflammation effect by inhibiting the NLRP3, thereby reducing the inflammation [49]. Figure 8(H-I) illustrates that the lung tissues of mice infused with BLM exhibited higher levels of NLRP3, and ASC protein when compared to the control groups ($p < 0.001$) and when treated with MV, the activity has been reduced, $p < 0.05$. The western blotting images obtained from the administration of MV significantly suppressed the expression of NLRP3, and ASC protein levels. This indicates that the drug is effective in mitigating PF. Numerous alarm signals, such as ATP, uric acid crystals, LPS, BLM, and different environmental irritants like asbestos, silica, and alum, can be detected by the NLRP3 in an inflammasome, which triggers an activation response. As a byproduct of NLRP3-induced macrophage activation, IL-1 β is essential for lung remodeling and fibrosis because it stimulates the production of pro-fibrotic mediators and activates fibroblasts, which leads to the deposition of collagen in the lung [21, 49]. This study aims to determine whether malvidin, a naturally occurring anthocyanin, can be used to treat mice's bleomycin-induced PF and NLRP3 inflammasome assembly. The main results point to malvidin's ability to considerably lessen NLRP3 inflammasome activation, which mitigates the fibrotic changes in lung tissue that bleomycin induces. These results highlight the need for more research to translate these findings into clinical practice and open up new avenues for malvidin as a novel therapeutic agent for fibrotic lung diseases.

Conclusion

This study demonstrates the therapeutic potential of MV in mitigating BLM-induced pulmonary fibrosis, a widely used model for investigating PF pathogenesis and evaluating novel treatments. MV alleviates oxidative stress by reducing ROS levels, enhancing the body's antioxidant defenses, inhibiting inflammatory pathways, and minimizing collagen deposition. As a result, it helps preserve lung structure and function while reducing PF severity.

The decline in HYP protein levels further supports MV's antifibrotic properties. By inhibiting TXNIP, MV lowers MDA, MPO, and CAT levels while increasing GSH and SOD levels, highlighting its antioxidant effects. Further preclinical and clinical studies are necessary to validate its therapeutic efficacy in human pulmonary fibrosis and other fibrotic conditions. MV offers a natural, multi-targeted approach to fibrosis treatment, addressing a crucial gap in current therapeutic options. This study enhances our understanding of PF mechanisms and introduces MV as a promising therapeutic candidate.

Supplementary Information

The online version contains supplementary material available at <https://doi.org/10.1186/s12950-025-00441-1>.

Supplementary Material 1.

Acknowledgements

None.

Authors' contributions

Linshen Xie: Writing – original draft, Visualization, Validation, Software, Methodology, Investigation, Conceptualization. Dingzi Zhou: Writing – review & editing, Lin Cai: Validation. Jie Xu: Data curation. Daigang Fu: Data curation. Ling Yan – Validation.

Funding

1. Supported by Sichuan Provincial Natural Science Foundation 2023NSFSC1730.
2. Supported by the Health Commission of Sichuan Province Medical Science and Technology Program 24QNMP072.

Data availability

No datasets were generated or analysed during the current study.

Declarations

Ethics approval and consent to participate

This research was approved by the animal ethical committee, Approved No. A2023NSFSC1730. All of the authors agree to work on this project.

Consent for publication

The approval of each author to publish the manuscript has been obtained. The manuscript is not currently under review by any other journal and has not been published before.

Competing interests

The authors declare no competing interests.

Received: 21 January 2025 / Accepted: 10 March 2025

Published online: 31 March 2025

References

1. Shariati S, Kalantar H, Pashmforosh M, Mansouri E, Khodayar MJ. Epicatechin protective effects on bleomycin-induced pulmonary oxidative stress and fibrosis in mice. *Biomed Pharmacother*. 2019;114:108776.
2. Moore BB, Hogaboam CM. Murine models of pulmonary fibrosis. *Am J Physiol Lung Cell Mol Physiol*. 2008;294(2):L152–60.
3. Lederer DJ, Martinez FJ. Idiopathic Pulmonary Fibrosis. Longo DL, editor. *New England Journal of Medicine* [Internet]. 2018;378:1811–23. Available from: <http://www.nejm.org/doi/https://doi.org/10.1056/NEJMra1705751>.
4. Martinez FJ, Safrin S, Weycker D, Starko KM, Bradford WZ, Talmadge; et al. The Clinical Course of Patients with Idiopathic Pulmonary Fibrosis Background: Prospective data defining the clinical course in [Internet]. 2005. Available from: www.annals.org.
5. Park SJ, Ryu HW, Kim JH, Hahn HJ, Jang HJ, Ko SK, et al. Daphnetin alleviates Bleomycin-Induced pulmonary fibrosis through Inhibition of Epithelial-to-Mesenchymal transition and IL-17A. *Cells*. 2023;12(24):2795.
6. Nalysnyk L, Cid-Ruzafa J, Rotella P, Esser D. Incidence and prevalence of idiopathic pulmonary fibrosis: review of the literature. *Eur Respiratory Rev*. 2012;21(126):355–61.
7. Bahramifar A, Jafari RM, Sheibani M, Manavi MA, Rashidian A, Tavangar SM, et al. Sumatriptan mitigates bleomycin-induced lung fibrosis in male rats: involvement of inflammation, oxidative stress and α -SMA. *Tissue Cell*. 2024;88:102349.
8. Moore BB, Lawson WE, Oury TD, Sisson TH, Raghavendran K, Hogaboam CM. Animal models of fibrotic lung disease. *Am J Respir Cell Mol Biol*. 2013;49(2):167–79.
9. Tzouveleki A, Harokopos V, Paparountas T, Oikonomou N, Chatziioannou A, Vilaras G, et al. Comparative expression profiling in pulmonary fibrosis suggests a role of hypoxia-inducible factor-1 α in disease pathogenesis. *Am J Respir Crit Care Med*. 2007;176:1108–19.
10. Bastin AR, Sadeghi A, Abolhassani M, Doustimotlagh AH, Mohammadi A. Malvidin prevents lipopolysaccharide-induced oxidative stress and inflammation in human peripheral blood mononuclear cells. *IUBMB Life*. 2020;72:1504–14.
11. Merez-Sadowska A, Sitarek P, Kowalczyk T, Zajdel K, Jęcek M, Nowak P, et al. Food anthocyanins: Malvidin and its glycosides as promising antioxidant and Anti-Inflammatory agents with potential health benefits. *Nutrients*. Multidisciplinary Digital Publishing Institute (MDPI); 2023.
12. Ma Y, Li Y, Zhang H, Wang Y, Wu C, Huang W. Malvidin induces hepatic stellate cell apoptosis via the Endoplasmic reticulum stress pathway and mitochondrial pathway. *Food Sci Nutr*. 2020;8:5095–106.
13. Ji J, Hou J, Xia Y, Xiang Z, Han X. NLRP3 inflammasome activation in alveolar epithelial cells promotes myofibroblast differentiation of lung-resident mesenchymal stem cells during pulmonary fibrogenesis. *Biochim Biophys Acta Mol Basis Dis*. 2021;1867(5):166077.
14. Gu W, Zeng Q, Wang X, Jasem H, Ma L. Acute lung injury and the NLRP3 inflammasome. *J Inflamm Res*. 2024;17:3801–13.
15. Tian R, Zhu Y, Yao J, Meng X, Wang J, Xie H, et al. NLRP3 participates in the regulation of EMT in bleomycin-induced pulmonary fibrosis. *Exp Cell Res*. 2017;357:328–34.
16. Yang Y, Wang H, Kouadir M, Song H, Shi F. Recent advances in the mechanisms of NLRP3 inflammasome activation and its inhibitors. *Cell Death Dis*. Nature Publishing Group; 2019.
17. Xie X, Wu X, Zhao D, Liu Y, Du Q, Li Y, et al. Fluvoxamine alleviates bleomycin-induced lung fibrosis via regulating the cGAS-STING pathway. *Pharmacol Res*. 2023;187.
18. Yang C, Xiong W, Dong J, Zhao X, Liang G, Zheng W. Artemisinin protected human bronchial epithelial cells from amiodarone-induced oxidative damage via 5'-AMP-activated protein kinase (AMPK) activation. *Redox Rep*. 2025;30(1):2447721.
19. Zhou L, Gao R, Hong H, Li X, Yang J, Shen W, et al. Emodin inhibiting neutrophil elastase-induced epithelial-mesenchymal transition through Notch1 signalling in alveolar epithelial cells. *J Cell Mol Med*. 2020;24:11998–2007.
20. Peng L, Wen L, Shi QF, Gao F, Huang B, Meng J, et al. Scutellarin ameliorates pulmonary fibrosis through inhibiting NF- κ B/NLRP3-mediated epithelial-mesenchymal transition and inflammation. *Cell Death Dis*. 2020;11(11):978.
21. Li Y, Li H, Liu S, Pan P, Su X, Tan H, et al. Pirfenidone ameliorates lipopolysaccharide-induced pulmonary inflammation and fibrosis by blocking NLRP3 inflammasome activation. *Mol Immunol*. 2018;99:134–44.
22. Wang J, Xiang Y, Yang SX, Zhang HM, Li H, Zong QB, et al. MIR99AHG inhibits EMT in pulmonary fibrosis via the miR-136-5p/USP4/ACE2 axis. *J Transl Med*. 2022;20(1):426.
23. Liang Q, Cai W, Zhao Y, Xu H, Tang H, Chen D, et al. Lycorine ameliorates bleomycin-induced pulmonary fibrosis via inhibiting NLRP3 inflammasome activation and pyroptosis. *Pharmacol Res*. 2020;158:104884.
24. Zhao P, Li X, Yang Q, Lu Y, Wang G, Yang H, et al. Malvidin alleviates mitochondrial dysfunction and ROS accumulation through activating AMPK- α /UCP2 axis, thereby resisting inflammation and apoptosis in SAE mice. *Front Pharmacol*. 2023;13:1038802.
25. Mohamed AS, Hosney M, Bassiony H, Hassanein SS, Soliman AM, Fahmy SR, et al. Sodium pentobarbital dosages for exsanguination affect biochemical, molecular and histological measurements in rats. *Sci Rep*. 2020;10(1):378.

26. Parasuraman S, Raveendran R, Kesavan R. Blood sample collection in small laboratory animals. *J Pharmacol Pharmacother*. 2010;1:87–93.
27. Farina F, Sancini G, Mantecca P, Gallinotti D, Camatini M, Palestini P. The acute toxic effects of particulate matter in mouse lung are related to size and season of collection. *Toxicol Lett*. 2011;202:209–17.
28. Li N, Wu K, Feng F, Wang L, Zhou X, Wang W. Astragaloside IV alleviates silica-induced pulmonary fibrosis via inactivation of the TGF- β 1/Smad2/3 signaling pathway. *Int J Mol Med*. 2021;47(3):16.
29. Kseibati MO, Sharawy MH, Salem HA. Chrysin mitigates bleomycin-induced pulmonary fibrosis in rats through regulating inflammation, oxidative stress, and hypoxia. *Int Immunopharmacol*. 2020;89:107011.
30. Lan YW, Chen YC, Yen CC, Chen HL, Tung MC, Fan HC, et al. Kefir peptides mitigate bleomycin-induced pulmonary fibrosis in mice through modulating oxidative stress, inflammation and gut microbiota. *Biomed Pharmacotherapy*. 2024;174:116431.
31. Zeyada MS, Eraky SM, El-Shishtawy MM. Trigonelline mitigates bleomycin-induced pulmonary inflammation and fibrosis: insight into NLRP3 inflammasome and SPHK1/S1P/Hippo signaling modulation. *Life Sci*. 2024;336:122272.
32. Adams EJ, Green JA, Clark AH, Youngson JH. Comparison of different scoring systems for immunohistochemical staining. *Clin Pathol*. 1999;52(1):75–7.
33. Sharawy MH, El-Agamy DS, Shalaby AA, Ammar ESM. Protective effects of Methyl palmitate against silica-induced pulmonary fibrosis in rats. *Int Immunopharmacol*. 2013;16:191–8.
34. Ali A, Mir GJ, Ayaz A, Maqbool I, Ahmad SB, Mushtaq S, et al. In Silico analysis and molecular Docking studies of natural compounds of *Withania somnifera* against bovine NLRP9. *J Mol Model*. 2023;29(6):171.
35. Vaidyanathan R, Murugan Sreedevi S, Ravichandran K, Vinod SM, Hari Krishnan Y, Babu LK, et al. Molecular Docking approach on the binding stability of derivatives of phenolic acids (DPAs) with human serum albumin (HSA): Hydrogen-bonding versus hydrophobic interactions or combined influences? *JCIS Open*. 2023;12:100096.
36. Lin J, Tian J, Shu C, Cheng Z, Liu Y, Wang W, et al. Malvidin-3-galactoside from blueberry suppresses the growth and metastasis potential of hepatocellular carcinoma cell Huh-7 by regulating apoptosis and metastases pathways. *Food Sci Hum Wellness*. 2020;9:136–45.
37. Quintieri AM, Baldino N, Filice E, Seta L, Vitetti A, Tota B, et al. Malvidin, a red wine polyphenol, modulates mammalian myocardial and coronary performance and protects the heart against ischemia/reperfusion injury. *J Nutr Biochem*. 2013;24:1221–31.
38. Andersson-Sjöland A, Karlsson JC, Rydell-Törmänen K. ROS-induced endothelial stress contributes to pulmonary fibrosis through pericytes and Wnt signaling. *Lab Invest*. 2016;96:206–17.
39. Gao F, Kinnula VL, Myllärniemi M, Oury TD. Extracellular superoxide dismutase in pulmonary fibrosis. *Antioxid Redox Signal*. 2008;10(2):343–54.
40. Huang W, Zhu Y, Li C, Sui Z, Min W. Effect of blueberry anthocyanins malvidin and glycosides on the antioxidant properties in endothelial cells. *Oxid Med Cell Longev*. 2016;2016:1591803.
41. Zhao F, Zhang YF, Liu YG, Zhou JJ, Li ZK, Wu CG, et al. Therapeutic effects of bone Marrow-Derived mesenchymal stem cells engraftment on Bleomycin-Induced lung injury in rats. *Transpl Proc*. 2008;40:1700–5.
42. El-Horany HES, Atef MM, Abdel Ghafar MT, Fouda MH, Nasef NA, Hegab II, et al. Empagliflozin ameliorates Bleomycin-Induced pulmonary fibrosis in rats by modulating Sesn2/AMPK/Nrf2 signaling and targeting ferroptosis and autophagy. *Int J Mol Sci*. 2023;24(11):9481.
43. Makena P, Kikalova T, Prasad GL, Baxter SA. Oxidative Stress and Lung Fibrosis: Towards an Adverse Outcome Pathway. *Int J Mol Sci. Multidisciplinary Digital Publishing Institute (MDPI)*; 2023.
44. Forman HJ, Zhang H. Targeting oxidative stress in disease: promise and limitations of antioxidant therapy. *Nat Rev Drug Discov Nat Res*; 2021;20(9):689–709.
45. Mao J, Yi M, Wang R, Huang Y, Chen M. Protective effects of Costunolide against D-Galactosamine and Lipopolysaccharide-Induced acute liver injury in mice. *Front Pharmacol*. 2018;9:1469.
46. Zhang X, Zhang W, Chen X, Cai Y. Prevention of Bleomycin-Induced Pulmonary Inflammation and Fibrosis in Mice by Bilobalide. *Evidence-based Complementary and Alternative Medicine*. 2023;2023.
47. Zou W, Zhang C, Gu X, Li X, Zhu H. Metformin in combination with Malvidin prevents progression of non-alcoholic fatty liver disease via improving lipid and glucose metabolisms, and inhibiting inflammation in type 2 diabetes rats. *Drug Des Devel Ther*. 2021;15:2565–76.
48. Gamad N, Malik S, Suchal K, Vasisht S, Tomar A, Arava S, et al. Metformin alleviates bleomycin-induced pulmonary fibrosis in rats: Pharmacological effects and molecular mechanisms. *Biomed Pharmacotherapy*. 2018;97:1544–53.
49. Fan H, Cui J, Liu F, Zhang W, Yang H, He N, et al. Malvidin protects against lipopolysaccharide-induced acute liver injury in mice via regulating Nrf2 and NLRP3 pathways and suppressing apoptosis and autophagy. *Eur J Pharmacol*. 2022;933:175252.

Publisher's Note

Springer Nature remains neutral with regard to jurisdictional claims in published maps and institutional affiliations.